IEEE Access
Multidisciplinary | Rapid Review | Open Access Journal

Received July 15, 2018, accepted August 21, 2018, date of publication August 27, 2018, date of current version September 21, 2018.

Digital Object Identifier 10.1109/ACCESS.2018.2867338

Cooperative Localization With Bounding Constraints in Mobile Wireless Sensor Networks

ZHAOYANG WANG[1], BAIHAI ZHANG[1], XIAOYI WANG[2], SENCHUN CHAI[1], AND YUTING BAI[1]

[1]Beijing Institute of Technology, Beijing 100081, China
[2]Beijing Technology and Business University, Beijing 100048, China

Corresponding author: Baihai Zhang (smczhang@bit.edu.cn)

This work was supported by the National Natural Science Foundations of China under Grant 61573061 and Grant 51179002.

ABSTRACT In mobile wireless sensor networks (WSNs), error accumulation, and outlier problem seriously decrease the localization accuracy. To find a more accurate and cost-effective localization algorithm, cooperative localization with bounding constraints is proposed in this paper. By depicting the factor graph, the cooperative localization combines the trajectory prediction and observation correction of adjacent node. The trajectory prediction utilizes the polynomial Newton interpolation and bounding box which avoid the gross error. The observation correction explores the belief propagation and variational message passing, which are improved by judgment factor and punctuation function. Experiments are conducted to verify the proposed method in the aspect of algorithm parameter configuration, experiment parameter configuration, and distribution parameter configuration. The experiment results show that the proposed method in this paper outperforms than existing methods in large-scale WSNs.

INDEX TERMS Cooperative localization, boundary box, mobile WSNs, massage passing.

I. INTRODUCTION

Mobile Wireless Sensor Networks (WSNs) find applications in environmental monitoring, space exploration and surveillance, etc [1], [2]. They comprise a number of sensor nodes which are deployed over a region and move at a random speed. Mobile WSNs only make sense when their locations are obtained. The localization of mobile WSNs needs to sequentially calculate the node position in real time. However, mobile WSNs avoid equipping more devices such as GPS considering the limitation of cost and energy. This requirement promotes the research on the localization accuracy and simplicity [3]–[7].

Many researches have been made on the localization of static WSNs. They are categorized into range-based and range-free methods. Range-based methods depend on the distance or angle measurement devices which are beneficial to higher localization accuracy, such as TOA, RSSI and AOA in Tomic's works [8], [9]. These methods have higher hardware cost and are not suitable for large-scale and complex networks. Range-free methods are not more accurate than range-based methods, but it avoids large hardware cost. These methods [10], [11] include DV-HOP, APIT and centroid which are more suitable for the scenario in this paper. However, methods above are only applied in static WSN. More and more sensors are equipped in vehicle or other mobile devices so that broader and more flexible monitoring can be realized. Due to the off-line operation and low real-time problems, these range-free methods above are not applied in mobile WSNs. In the paper, we explore the localization for mobile WSNs.

For localization of mobile WSNs, Monte Carlo is the most popular method which is initially proposed by Hu and Evans [12]. Without additional hardware, sequential Monte Carlo Localization predicts the position area and filters by importance sampling. This technique studies range-free localization in the presence of mobility and improves the accuracy. On the basis of MCL, Baggio *et al.* constrain the area where samples are drawn by building a box. The radio ranges of anchors in the box overlap [13]. The box method is called Monte Carlo localization boxed (MCB). MCB draws the necessary location samples faster so that the accuracy and efficiency are improved. Besides, MSL [14], MSL* [15], MMCL [13], RSS-MCL [16] and OTMCL [17] are all improved MCL. For improved MCL, Guan *et al.* [18] propose an optimal region selection strategy of Voronoi diagram based on VMCL, called ORSS-VMCL. It increases the efficiency

and accuracy for VMCL by adapting the size of Voronoi area during the filtering process. Rashid and Turuk [19] propose a technique called dead reckoning localization for mobile WSNs (DRLMSN). It estimates two possible locations of a node using Bézout's theorem. A dead reckoning approach is used to select one of the two estimated locations. Wang and Zhu [16] sequentially estimate the location of mobile nodes, using the log-normal statistical model of RSS measurement. The RSS measurement is treated as the observation model in Monte Carlo method and the mobility feature of nodes as the transition model. The MCL and its improvements decrease the hardware cost and operate conveniently while they are limited by unsuccessful sampling and particle degeneracy. The unsuccessful sampling and particle degeneracy add extra computation and decrease the localization accuracy. The problems limit the development of MCL in mobile WSN localization.

As implementations of approximate Bayesian inference, cooperative localization enhances the technique in WSN localization [20], [21]. The cooperative localization develops initially in static WSNs. Nguyen *et al.* [22] study least square (LS) cooperative localization in the presence of arbitrary non-line-of-sight (NLOS) ranging bias and derive the Fisher information matrix (FIM) for a general NLOS bias model. Li and Hedley [23] propose an asymmetric double exponential ranging error model based on empirical ranging data. The communication and computational cost is reduced by Gaussian distributions between neighbors and by using an analytical approximation to compute peer-to-peer messages. García-Fernández *et al.* [24] presents the posterior linearization belief propagation (PLBP) algorithm for cooperative localization with linearization and belief propagation. At the linearization step, the nonlinear functions are linearized using statistical linear regression with respect to the current beliefs. Cooperative methods above have good performance in localization of static WSNs, but they are not applicable in mobile WSNs. Mobile WSNs faces the movement of anchors and unknown nodes. The position changes overtime which would result in the uncertainty and randomness. The uncertainty and randomness are not considered in the static localization methods. Besides, the computation complexity of static localization doesn't meet the requirement of real-time. These problems need to be considered in mobile WSN localization.

To solve the problems in mobile WSNs, dynamic cooperative localization methods are proposed and improved accordingly. Wymeersch et al. initially extended message passing in mobile WSNs. The cooperative problem is transformed as marginal function estimation called Sum-Product Algorithm over a Wireless Networks (SPAWN) [25]–[27]. For robustness, Wymeersch optimizes the edge as a variable in factor graph and proposes Uniformly Reweighted Belief Propagation (URWBP) [28], [29]. Localizations above obtain high accuracy, but the high computational complexity and large communication overhead are neglected. Pedersen and Das focus on the problem and propose Variational Message Passing (VMP) and Cramér Rao Bound (CRB) respectively. By selecting the transmission and message form, the large communication overhead and communication link are effectively reduced [30], [31]. Li and Cui explore the Gaussian message in the application of communication which introduces first-order or second-order Taylor expansion. This message form combined by belief propagation (BP) and VMP linearizes ranging model and control communication overhead and computational complexity [32]–[34]. The cooperative process in papers above corrects the position error macroscopically, but it faces the problem of error accumulation. As nodes move with time, the localization error in the last time impacts on the localization process later. The error accumulation may lead to the position deviation of whole networks. To avoid the error accumulation, researchers engage in decreasing error from the source. Improving the measurement accuracy is a way to decrease the error from the source, so many range-based methods are adopted to decrease the measurement error. Çakmak and Urup employ Belief propagation and mean field message passing for the motion-related and measurement-related parts of the factor graph [35]. Yuan et al. present a factor graph (FG) representation of joint localization and time synchronization problem based on TOA measurements [36]. These researches have been widely used in cooperative localization, but the contradiction still affects the performance. In the large-scale and complex WSNs, the hardware cost is firstly considered. Although the cooperative localization outperforms in accuracy, it highly depends on the hardware. The WSNs need to equip more speed and distance measurement devices which cause extra cost. However, the cost and accuracy are the main contradiction. Another way to impact on the accuracy is the outlier problem. Although range-based method improves measurement accuracy, it still can't avoid the outlier measurement. Due to the NLOS or the existence of malicious node, outlier emerges and it isn't calibrated. The outlier problem can lead to catastrophic problem. It disrupts estimated topology of WSNs, and finally the localization fails.

In our paper, we mainly focus on the large-scale and complex scenario of WSNs, so the cost is strictly limited. Without equipping speed and distance measurement devices, the node distance and position prediction is only estimated by topological structure and maximum speed. For node trajectory prediction, the Newton Interpolation preliminarily estimates the node position of next time. It can replace speed measurement devices, but the imprecise estimation result may lead to error accumulation and big deviation. To solve the problem, we propose the bounding box to restrict the prediction area by maximum speed and communication radius. These initial positions of nodes affect the localization of other nodes by distance. Cooperative localization takes advantage of these characteristics in which the node distance is estimated by multi-hop algorithm without extra hardware cost. Among the prediction message, the cooperative localization coordinates by BP update rule. Among the observation message, the cooperative localization coordinates by VMP update rule. To avoid the error accumulation, we introduce the punctuation function

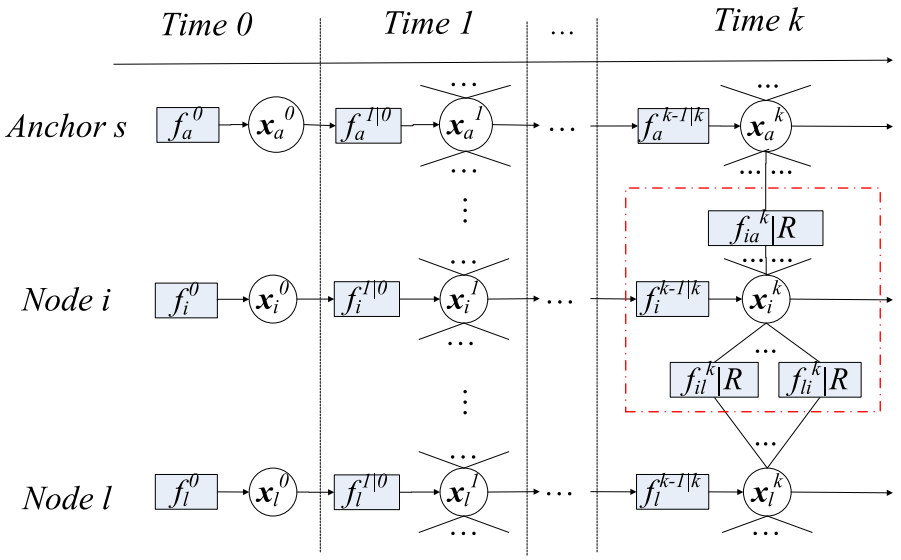

FIGURE 1. Factor graph.

and judgment factor. These improvements approach the real position more after iterated localization.

II. PROBLEM FORMATION AND SYSTEM MODEL

WSNs consist of anchor set A and unknown node set M which are uniformly deployed in 2D space. The anchors obtain their own position by equipping devices. The unknown nodes cannot obtain their own position and have to estimate position relying on anchors. The anchor set A and unknown node set M are denoted as node set $H = A \cup M$. All nodes move within the maximum speed $\mathbf{v}_{\max}$. Since time is slotted, positions of nodes are denoted by $\mathbf{x}_i^k \triangleq \left[x_{i1}^k, x_{i2}^k\right]^T$. Their position sets are defined as $\mathbf{X} \triangleq \left\{\mathbf{x}_i^k : i \in H\right\}$. In particular, for an anchor $a \in A$, its position is denoted as $\boldsymbol{\mu}_i^k \triangleq \left[\mu_{i1}^k, \mu_{i2}^k\right]^T$. For all time slots, the position set is $\mathbf{X}^{0:K} \triangleq \left\{\mathbf{X}^0, \mathbf{X}^1, \cdots, \mathbf{X}^K\right\}$. Assuming the node moves from time $k-1$ to time k at the speed $\mathbf{v}_i^k$, the state transition model of sensor i at the *kth* time slot is formulated as

$$\mathbf{x}_i^k = \mathbf{x}_i^{k-1} + \mathbf{v}_\mathbf{i}^\mathbf{k} \cdot \Delta T + \mathbf{e}_i^k \tag{1}$$

Where $\mathbf{e}_i^k \sim N\left(\mathbf{e}_i^k; 0, \mathbf{V}_{e_i^k}\right)$ is the system noise, ΔT is the time interval. The probabilistic state-transition function is shown in formula (2).

$$p\left(\mathbf{x}_i^k \left| \mathbf{x}_i^{k-1}\right.\right) = N\left(\mathbf{x}_i^k; \mathbf{x}_i^{k-1} + \mathbf{v}_\mathbf{i}^\mathbf{k} \cdot \Delta T, \mathbf{V}_{e_i^k}\right) \tag{2}$$

For all nodes which are assumed to be independent, the joint state-transition function is shown in formula (3).

$$p\left(\mathbf{X}^k \left| \mathbf{X}^{k-1}\right.\right) = \prod_{i \in V} p\left(\mathbf{x}_i^k \left| \mathbf{x}_i^{k-1}\right.\right) \tag{3}$$

As the observation value, node distance at time slot k is denoted as $\mathbf{Z}^k \triangleq \left\{\mathbf{d}_{i \leftarrow j}^k : i \in H, j \in H_i^k\right\}$, where H_i^k denotes all the neighboring nodes around node i at time slot k. For all time slots, the node distance set is defined as $\mathbf{Z}^{1:k} \triangleq \left\{\mathbf{Z}^1, \mathbf{Z}^2, \cdots, \mathbf{Z}^k\right\}$. Each node measures its distance with neighboring nodes as expressed in formula (4).

$$\mathbf{d}_{i \leftarrow j}^k = \left\|\mathbf{x}_i^k - \mathbf{x}_j^k\right\| + e_{ij}^k \tag{4}$$

Where, $\|\cdot\|$ denotes the Euclidean norm and e_{ij}^k is the range measurement error. Its probability density function is shown in formula (5).

$$p\left(\mathbf{d}_{i \leftarrow j}^k \left| \mathbf{x}_i^k, \mathbf{x}_j^k\right.\right) = \frac{1}{\sqrt{2\pi\left(\sigma_{ij}^k\right)^2}} \exp\left\{-\frac{\left(\mathbf{d}_{i \leftarrow j}^k - \left\|\mathbf{x}_j^k - \mathbf{x}_i^k\right\|\right)^2}{2\left(\sigma_{ij}^k\right)^2}\right\} \tag{5}$$

Where σ_{ij}^k is the standard deviation of distance between node i and j in time slot t_k. The standard deviation is related to the accuracy of distance measurement. Assuming that distance measurement is independent, the observation probability function is shown in formula (6).

$$p\left(\mathbf{Z}^k \left| \mathbf{X}^k\right.\right) = \prod_{i \in M} \prod_{j \in H_i^k} p\left(\mathbf{d}_{i \leftarrow j}^k \left| \mathbf{x}_i^k, \mathbf{x}_j^k\right.\right) \tag{6}$$

On the basis of Bayesian rules, the joint posteriori distribution of $\mathbf{X}^{0:K}$ with given observations $\mathbf{Z}^{0:K}$ is shown in formula (7).

$$\begin{aligned} p\left(\mathbf{X}^{0:K} \left| \mathbf{Z}^{1:K}\right.\right) &\propto p\left(\mathbf{X}^{0:K}\right) p\left(\mathbf{Z}^{1:K} \left| \mathbf{X}^{0:K}\right.\right) \\ &= p\left(\mathbf{X}^0\right) \prod_{k=1}^{K} p\left(\mathbf{X}^k \left| \mathbf{X}^{k-1}\right.\right) p\left(\mathbf{Z}^k \left| \mathbf{X}^k\right.\right) \end{aligned} \tag{7}$$

As a graph model, factor graph describes the relationship between variables and factors by factorization of a global

function. WSNs can be abstracted as a graph model where every local function is denoted by a factor node, and each variable is denoted by an edge or half-edge. The factor graph of WSNs is shown in FIGURE 1 and their definitions are $f_i^k \triangleq p\left(\mathbf{x}_i^k\right), f_i^{k|k-1} \triangleq p\left(\mathbf{x}_i^k \left| \mathbf{x}_i^{k-1}\right.\right), f_{ij}^k \triangleq p\left(d_{i\leftarrow j}^k \left| \mathbf{x}_i^k, \mathbf{x}_j^k\right.\right)$.

III. TRAJECTORY PREDICTION AND BOUNDING BOX

A. TRAJECTORY PREDICTION

The localization of mobile WSNs consists of prediction message from historical trajectory and cooperative message from observation value. We firstly calculate prediction message. Considering hardware cost, WSNs don't equip the speed measurement device thus they cannot obtain the speed in real time. With the maximum speeds only known, Polynomial Newton Interpolation predicts the node trajectory through historical trajectory.

Polynomial Newton Interpolation is an important method of function approximation, and it has been widely used. When it predicts the node trajectory, the Polynomial Newton Interpolation has less computation complexity and resource occupancy. Besides, Polynomial Newton Interpolation analyzes the node movement trend and characteristics with less historical data and better predict the node trajectory. Because mobile WSN is real-time system, it strictly restricts the computation time and storage space. These requirements can be met by Polynomial Newton Interpolation.

Polynomial Newton Interpolation predicts the node position by depicting the trend curve of node movement, so interpolation function of trajectory is firstly calculated. The prediction position after interpolation is shown in formula (8).

$$\mathbf{x}_k = f(t) = N\mathbf{x}_{k-1}(t) + R\mathbf{x}_{k-1}(t) \tag{8}$$

Where $N\mathbf{x}_{k-1}(t)$ is the interpolation formula and $R\mathbf{x}_{k-1}(t)$ is the remainder. In formula (8), $N\mathbf{x}_{k-1}(t)$ denotes the trajectory of node movement. While the interpolation result must have deviation from true trajectory, the remainder $R\mathbf{x}_{k-1}(t)$ is introduced to denote the deviation. The remainder has little influence on the interpolation result, but it denotes the deviation range. As long as the deviation is acceptable for trajectory prediction, the order of interpolation is determined. Because localization of Message Passing can correct the position of unknown node, the trajectory is not required to reach high accuracy. Meanwhile, to avoid increasing computation and resource occupancy, the interpolation hopes to find the simplest way to predict trajectory. The quadratic interpolation is introduced considering that its prediction process is as simple as possible. The last three groups of historical data form the interpolation formula and remainder which are shown in (9) and (10).

$$\begin{aligned} N\mathbf{x}_{k-1}(t) = {} & f(t_{k-3}) + f[t_{k-3}, t_{k-2}](t_{k-3} - t_{k-2}) \\ & + f[t_{k-3}, t_{k-2}, t_{k-1}](t - t_{k-3})(t - t_{k-2}) \end{aligned} \tag{9}$$

$$R\mathbf{x}_{k-1}(t) = f[t, t_{k-3}, t_{k-2}, t_{k-1}](t-t_{k-3})(t-t_{k-2})(t-t_{k-1}) \tag{10}$$

Where t is the time of the $k-th$ localization. t_{k-1}, t_{k-2}, t_{k-3} are the time of $(k-1)\,th$, $(k-2)\,th$, $(k-3)\,th$ localization.

$f(t_{k-3}, t_{k-2})$, $f[t_{k-3}, t_{k-2}, t_{k-1}]$, $f[t, t_{k-3}, t_{k-2}, t_{k-1}]$ are the interpolation coefficients. Its calculation is shown in formula (11) to (13).

$$f(t_k) = \mathbf{x}_k, \quad f(t_{k-3}, t_{k-2}) = \frac{f(t_{k-3}) - f(t_{k-2})}{t_{k-3} - t_{k-2}} \tag{11}$$

$$f[t_{k-3}, t_{k-2}, t_{k-1}] = \frac{f[t_{k-3}, t_{k-2}] - f[t_{k-2}, t_{k-1}]}{t_{k-3} - t_{k-1}} \tag{12}$$

$$f[t, t_{k-3}, t_{k-2}, t_{k-1}] = \frac{f[t, t_{k-3}] - f[t_{k-3}, t_{k-2}] - f[t_{k-2}, t_{k-1}]}{t - t_{k-3}} \tag{13}$$

In formula (11), (12) and (13), the interpolation coefficients are calculated by historical trajectory. The historical data of position depicts the curve of trajectory so that position of next time is determined by the trajectory trend. As shown in the formula, $f(t_k)$ is the position of kth localization. The divided differences $f(t_{k-3})$, $f[t_{k-3}, t_{k-2}]$, $f[t_{k-3}, t_{k-2}, t_{k-1}]$ are analyzed by the latest three historical data which finally deduce the prediction result.

B. BOUNDING BOX

The prediction message from Polynomial Newton Interpolation is inaccurate which may cause large deviation due to error accumulation. This problem is corrected by introducing bounding box. Bounding box depict the possible range where the unknown node may locate. When the predicted position seriously deviate the possible range, the bounding box realize the calibration without extra computation. The size of bounding box is smaller; the accuracy of localization is higher.

The bounding box refers to the building of Monte Carlo Box (MCB) with only two hops range considered. At time slot k, the unknown nodes receive the transmitting signal power to distinguish that the anchor is within or outside the communication radius. If the unknown node receives the signal, the unknown node is within the communication radius of anchor. If not, the unknown node is outside the communication radius of anchor. Then, unknown nodes record the anchors within the communication radius and pack them as messages. These messages are sent to other unknown nodes. Other unknown nodes fuse the information with their own judgment information and distinguish the anchors within two-hop range. As shown in FIGURE 2, the area in which node can communicate with the anchor is a circle, but intersection of several circles is difficult to solve by mathematical deduction. To simplify the mathematical representation of intersection, the communication range is denoted by square. Considering omission of possible area, the whole circle should be in the square. Anchors within two-hop range are regarded as the center. Quadruplicate communication radius is regarded as the border length of square. FIGURE 2 shows three anchors and their

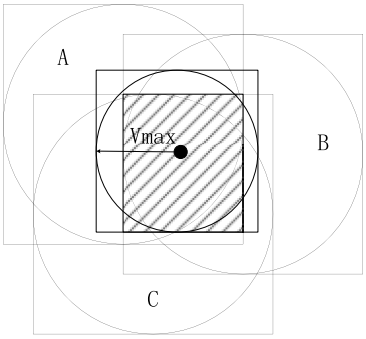

FIGURE 2. Bounding box.

communication ranges. The intersection of three squares is a rectangle called anchor box. Anchor box denotes the possible area in which node can communicate with three anchors. The bounding of anchor box is shown in formula (14).

$$\begin{cases} x_{1\min} = \max_{j=1}^{n} \left(x_{1j} - R\right) \\ x_{1\max} = \min_{j=1}^{n} \left(x_{1j} + R\right) \\ x_{2\min} = \max_{j=1}^{n} \left(x_{2j} - R\right) \\ x_{2\max} = \min_{j=1}^{n} \left(x_{2j} + R\right) \end{cases} \tag{14}$$

Where $x_{1\min}, x_{1\max}$ denote the upper bound and lower bound of x_1 direction, and $x_{2\min}, x_{2\max}$ denote the upper bound and lower bound of x_2 direction. (x_{1j}, x_{2j}) denotes the coordinate of *jth* anchor. R is the communication radius.

Besides, the position in previous time and maximum speed also restrict the predicting position. If the node moves with the speed no more than $2V_{\max}$, it must locate in the circle area. In the same way, the circle is difficult to denote its bounding by mathematical formula, so the restriction is also denoted by square. The square is drawn with the position x_{k-1} in last time as the center and $2V_{\max}$ as border length respectively. This square's intersection with anchor box is the bounding box as shown in FIGURE 2. The bounding box depicts the possible area where unknown node may locate. Its bounding is shown in formula (15).

$$\begin{cases} x_{1\min} = \max\left(x_{1\min}, x_{1(k-1)} - V_{\max}\right) \\ x_{1\max} = \min\left(x_{1\max}, x_{1(k-1)} + V_{\max}\right) \\ x_{2\min} = \max\left(x_{2\min}, x_{2(k-1)} - V_{\max}\right) \\ x_{2\max} = \min\left(x_{2\max}, x_{2(k-1)} + V_{\max}\right) \end{cases} \tag{15}$$

Where $\mathbf{V}_{\max}$ is the maximum speed of node movement. $(x_{1(k-1)}, x_{2(k-1)})$ is the coordinate when the time is t_{k-1}.

However, the bounding box doesn't consider the difference between one-hop anchor and two-hop anchor. To further exact the bounding box, the bounding box narrows the area through difference of one-hop and two-hop distance. In FIGURE 3, the shadow part is the area where node can communicate with the anchor directly. The white part is the area where node can communicate with the anchor thought one forwarding node. Once the unknown node isn't in the one-hop distance, the bounding box excludes the shadow part as shown in FIGURE 3. It is the area for anchor within two-hop range

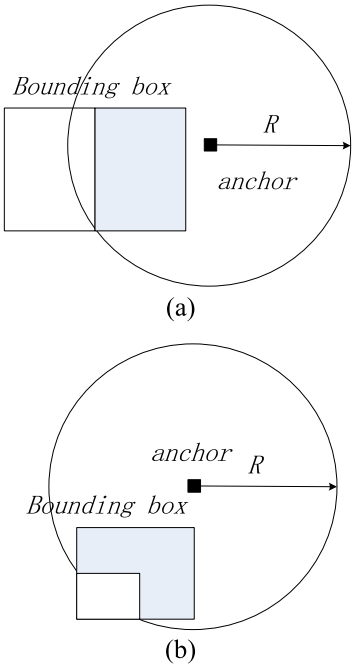

FIGURE 3. Exclusion of shadow area. (a) Two angles of rectangle in the circle. (b) Three angles of rectangle in the circle.

and beyond one-hop range. From FIGURE 3(a), two angles of rectangle are in the circle. The initial bounding box cuts the shadow area and forms a more accurate bounding box. FIGURE 3(b) shows the situation where three angles are in the circle. The initial bounding box cuts the shadow area and forms a new bounding box. These two situations follow the rules that the possible position of unknown nodes cannot be cut. The square in which only one angle is in the circle don't need cut.

The bounding box describes all the possible positions of unknown node through communication information. If the predicted position is outside the bounding box, it means the predicted position has large deviation from real position. Therefore, the predicted position should be calibrated. Because the bounding box includes all the possible positions, the calibrated position should be selected in the bounding box. Based on the error minimum, the center of bounding box is regarded as the predicted position instead of the position from Polynomial Newton Interpolation. If the predicted position is in the bounding box, the position from Polynomial Newton Interpolation is not changed. In the condition, the bounding box corrects the prediction result of Polynomial Newton Interpolation so that large deviation is avoided.

IV. COOPERATIVE LOCALIZATION

A. DISTANCE ESTIMATION

To save the cost and avoid distance measurement devices, we introduce the multi-hop algorithm to estimate the node distance. Compared with range-based distance measurement, the multi-hop algorithm doesn't need any hardware devices. To some extent, it saves the hardware cost.

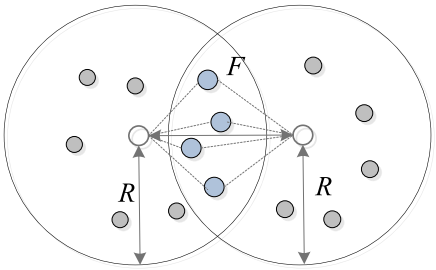

FIGURE 4. Two-hop node distance estimation.

At the same time, it has higher accuracy in distance estimation than DV-HOP, etc. The accurate distance obtained contributes to localization. Therefore, multi-hop algorithm is adopted in cooperative localization especially in large scale WSNs.

The formula of node distance is shown in formula (16).

$$\mathbf{d}_{i\leftarrow j} \approx \sum_{l=1}^{n_h} h_l \tag{16}$$

Where h_l denotes the *lth* hop distance.

On the shortest path, two-hop distance, one unit, is firstly calculated as shown in FIGURE 4. The reasons for selecting two-hop distance estimation reflect in two ways. Two-hop distance estimation reduces the computation by half. If one unit is two-hop, the unit number is less than that of hops between two nodes. The distance computation of units is reduced. This approach avoids repeated and redundant computation. On the other hand, Two-hop distance estimation has larger coverage area with double communication radius. Based on analysis of probability, larger area covers more nodes which reduce the uncertainty and randomness. Regarding two hops as one unit improves the accuracy of distance estimation. Therefore node distance estimation introduces the two-hop distance estimation, and only when the shortest path is odd, is the last hop distance calculated by one-hop distance estimation. The intersection of two circles is denoted as $F = D_k(R) \cap S_i(R)$. Its relationship with node distance is shown in formula (17).

$$F = \phi(\mathbf{d}_{i\leftarrow k}) = 2R^2 \cos^{-1}\left(\frac{\mathbf{d}_{i\leftarrow k}}{2R}\right) - \frac{1}{2}\mathbf{d}_{i\leftarrow k}\sqrt{4R^2 - \mathbf{d}_{i\leftarrow k}^2} \tag{17}$$

Where $\phi(d)$ is a decreasing function about distance $d_{i\leftarrow k}$ which is obtained by $F = m/(N/S)$. We assume that WSN environment has low level of interference associate to WSN signal. Each node can communicate with accurate number of nodes. In the condition, N is the number of nodes. S is the node distribution area. N/S is the node density. m is the number of node in the specific area. The node distance is denoted as formula (18).

$$\widehat{\mathbf{d}_{\mathbf{i}\leftarrow\mathbf{k}}} = \psi\left(\widehat{F}\right) \tag{18}$$

In formula (18), the closed loop solution cannot be obtained. To solve the problem, Secant method $\widetilde{\phi}(x) = \phi(x) - \widehat{F}$ looks for the solution by iteration shown in (19).

$$\widehat{\mathbf{d}}_{i\leftarrow k}^{p+1} = \widehat{\mathbf{d}}_{i\leftarrow k}^{p} - \widetilde{\phi}\left(\mathbf{d}_{i\leftarrow k}^{p}\right)\frac{\mathbf{d}_{i\leftarrow k}^{p} - \mathbf{d}_{i\leftarrow k}^{p-1}}{\phi\left(\mathbf{d}_{i\leftarrow k}^{p}\right) - \phi\left(\mathbf{d}_{i\leftarrow k}^{p-1}\right)} \tag{19}$$

Where p denotes the iteration times. Its convergence condition is $p = p^{\max} = \inf_p\left\{\widehat{\mathbf{d}}_{i\leftarrow k}^{p} = \widehat{\mathbf{d}}_{i\leftarrow k}^{p+s}, \forall s \in N^*\right\}$. To obtain $\widehat{\mathbf{d}}_{i\leftarrow k}^{p} = \widehat{\mathbf{d}}_{i\leftarrow k}^{p^{\max}}$, we set $\widehat{\mathbf{d}}_{i\leftarrow k}^{0} = R$, $\widehat{\mathbf{d}}_{i\leftarrow k}^{1} = 2R$.

If the hops are even on the shortest path, the node distance is shown in formula (20).

$$\hat{\mathbf{d}}_{i\leftarrow k} = \sum_{l=1}^{n_h/2} \Psi\left(\frac{m_l}{\lambda}\right) \tag{20}$$

If the hops are odd on the shortest path, the node distance is shown in formula (21).

$$\hat{\mathbf{d}}_{i\leftarrow k} = \sum_{l=1}^{(n_h-1)/2} \Psi\left(\frac{m_l}{\lambda}\right) + \mathbf{d}_{av}^{Last} \tag{21}$$

The distance of last hop d_{av}^{Last} follows the calculation of two-hop distance as shown in FIGURE 5. The relationship of intersection and node distance is denoted as formula (22).

$$\begin{aligned}\frac{A(s_k)}{A(s_j)} &= f\left(\mathbf{d}_{k\leftarrow j}\right) \\ &= \frac{\pi R^2}{2\cos^{-1}\left(\mathbf{d}_{k\leftarrow j}/2R\right) - \mathbf{d}_{k\leftarrow j}\sqrt{R^2 - \mathbf{d}_{k\leftarrow j}^2/4}} - 1\end{aligned} \tag{22}$$

Where $A(s_k)$ and $A\left(s_j\right)$ are the area of s_k, s_j. Their proportion can be also denoted by the neighboring number as shown in formula (23).

$$f\left(\mathbf{d}_{k\leftarrow j}\right) \approx \frac{\left|N(s_k) - N\left(s_j\right)\right|}{\left|N(s_k) \cap N\left(s_j\right)\right|} \tag{23}$$

Where $N(s_k)$, $N\left(s_j\right)$ are the number of node in area s_k, s_j.

As the calculation of two-hop distance, Secant method solves the node distance of last hop as shown in formula (24).

$$\mathbf{d}_{k\leftarrow j} \approx f^{-1}\left(\frac{\left|N(s_k) - N\left(s_j\right)\right|}{\left|N(s_k) \cap N\left(s_j\right)\right|}\right) \tag{24}$$

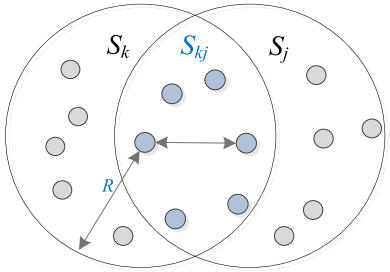

FIGURE 5. Last hop node distance estimation.

B. COOPERATIVE LOCALIZATION

The position from prediction phase is far from accuracy requirement. Because the positions of all nodes and the estimated distance are fuzzy, the estimated positions of unknown nodes are fuzzy and uncertain. The fuzziness and uncertainty may lead to the error propagation and accumulation especially in time varying system. To solve the problem, the fuzziness and uncertainty are reflected in the factor graph which is processed by Massage Passing. Massage Passing is a cooperative localization method. It overcomes the benchmark lack problem, lowers the requirement of node emission power and improves the usability, robustness and accuracy of localization.

The observation value of node distance adjusts the node position to approach the real position which has been reflected in factor graph. From the factor graph, messages are categorized into prediction message and cooperative message. The prediction message belongs to internal message. The cooperative message belongs to internode message. Due to the linearity of internal message, BP update rule is introduced in prediction phase. Considering non-linear ranging model, VMP update rule computes the cooperative message in correction phase.

In prediction phase, BP update rule is shown in formula (25).

$$\mathbf{m}_{f_i^{k|k-1}\to\mathbf{x}_i^k}\left(\mathbf{x}_i^k\right) = \int p\left(\mathbf{x}_i^k\left|\mathbf{x}_i^{k-1}\right.\right)\mathbf{m}_{\mathbf{x}_i^{k-1}\to f_i^{k|k-1}}\left(\mathbf{x}_i^{k-1}\right)d\mathbf{x}_i^{k-1} \quad (25)$$

Where $\mathbf{m}_{f_i^{k|k-1}\to\mathbf{x}_i^k}\left(\mathbf{x}_i^k\right)$ is the message from factor node $f_i^{k|k-1}$ to variable node $\mathbf{x}_i^k$ as shown in FIGURE 1. $\mathbf{m}_{\mathbf{x}_i^{k-1}\to f_i^{k|k-1}}$ is message from variable node $\mathbf{x}_i^{k-1}$ to factor node $f_i^{k|k-1}$.

In correction phase, VMP update rules including the anchors and unknown nodes are shown in formula (26) and (27).

$$\mathbf{m}_{f_{ia}^k\to\mathbf{x}_i^k}\left(\mathbf{x}_i^k\right) = \exp\left(\int b\left(\mathbf{x}_a^k\right)\ln p\left(\mathbf{d}_{i\leftarrow a}^k\left|\mathbf{x}_i^k,\mathbf{x}_a^k\right.\right)d\mathbf{x}_a^k\right) \quad (26)$$

$$\mathbf{m}_{f_{il}^k\to\mathbf{x}_i^k}\left(\mathbf{x}_i^k\right) = \exp\left(\int b\left(\mathbf{x}_l^k\right)\ln p\left(\mathbf{d}_{i\leftarrow l}^k\left|\mathbf{x}_i^k,\mathbf{x}_l^k\right.\right)d\mathbf{x}_l^k\right) \quad (27)$$

Similarly, $\mathbf{m}_{f_{ia}^k\to\mathbf{x}_i^k}\left(\mathbf{x}_i^k\right)$ is the message from factor node f_{ia}^k to variable node $\mathbf{x}_i^k$ as shown in FIGURE 1. This message is the information from neighboring anchors. $\mathbf{m}_{f_{il}^k\to\mathbf{x}_i^k}\left(\mathbf{x}_i^k\right)$ is the message from factor node f_{il}^k to variable node $\mathbf{x}_i^k$. This message is the information from neighboring unknown nodes. $b\left(\mathbf{x}_a^k\right)$ is the confidence of anchor a at time k. $b\left(\mathbf{x}_l^k\right)$ is the confidence of unknown node l at time k.

As shown in VMP update rule, the small error in initial computation may lead to error accumulation and trajectory drift. To solve the problem, we define the punctuation function and judgment factor to improve the VMP update rule. The redefined VMP update rule is shown in formula (28) and (29).

$$\mathbf{m}_{f_{ia}^k\to\mathbf{x}_i^k}\left(\mathbf{x}_i^k\right) = P_{f_{ia}^k\to\mathbf{x}_i^k}\left(\mathbf{x}_i^k\right)\exp\left(\int\theta\left(J_a^R\right)b\left(\mathbf{x}_a^k\right)\times\ln p\left(\mathbf{d}_{i\leftarrow a}^k\left|\mathbf{x}_i^k,\mathbf{x}_a^k\right.\right)d\mathbf{x}_a^k\right) \quad (28)$$

$$\mathbf{m}_{f_{il}^k\to\mathbf{x}_i^k}\left(\mathbf{x}_i^k\right) = P_{f_{il}^k\to\mathbf{x}_i^k}\left(\mathbf{x}_i^k\right)\exp\left(\int\theta\left(J_l^R\right)b\left(\mathbf{x}_l^k\right)\times\ln p\left(\mathbf{d}_{i\leftarrow l}^k\left|\mathbf{x}_i^k,\mathbf{x}_l^k\right.\right)d\mathbf{x}_l^k\right) \quad (29)$$

Where $\theta\left(J_a^R\right)$ and $\theta\left(J_l^R\right)$ are judgment factor. $\theta\left(J_a^R\right)$ focuses on the communication radius. After each iteration is completed, the renewed position of unknown node with neighboring anchors may be in the communication radius or not. If the renewed position meets the real relationship of communication radius, $\theta\left(J_a^R\right)=1$. If not, $\theta\left(J_a^R\right)=0$. $\theta\left(J_l^R\right)$ has the same condition with $\theta\left(J_a^R\right)$. If the renewed position meets the real relationship of communication radius, $\theta\left(J_l^R\right)=1$. If not, $\theta\left(J_a^R\right)=0$. $P_{f_{ia}^k\to\mathbf{x}_i^k}\left(\mathbf{x}_i^k\right)$ is the punctuation function defined as $P_{f_{ia}^k\to\mathbf{x}_i^k}\left(\mathbf{x}_i^k\right)=\exp\left(\delta v_i\left(\mathbf{x}\right)\right)$. $v_i\left(\mathbf{x}\right)$ denotes the node number change which accords with relationship of communication radius. After the position is renewed, judgment should be conducted. If the nodes according with the condition are added, $v_i\left(\mathbf{x}\right)=1$. If not, $v_i\left(\mathbf{x}\right)=p/q$ where p denotes the eligible node number after the position is renewed. p denotes the eligible node number before the position is renewed. δ is the floating constant which describes the influence of eligible node number.

After combining all internal messages and internode message, the node confidence is shown in formula (30).

$$b\left(\mathbf{x}_i^k\right)\triangleq\frac{1}{Z}\mathbf{m}_{f_i^{k|k-1}\to\mathbf{x}_i^k}\left(\mathbf{x}_i^k\right)\prod_{a\in A_i^k}\mathbf{m}_{f_{ia}^k-\mathbf{x}_i^k}\left(\mathbf{x}_i^k\right)\times\prod_{l\in M_i^k}\mathbf{m}_{f_{il}^k-\mathbf{x}_i^k}\left(\mathbf{x}_i^k\right) \quad (30)$$

Where Z is the confidence constant.

In this situation, the confidence computation has large communication load. To lower complexity, we further deduce the confidence estimation with punctuation function and judgment factor. Refining the formula (30), the confidence formula is transformed to formula (31).

$$b\left(\mathbf{x}_i^k\right)\propto\exp\left\{g_{k|k-1}\left(\mathbf{x}_i^k\right)+\delta V_a\left(\mathbf{x}\right)\sum_{a\in A_i^k}\theta\left(J_a^R\right)g_{ia}\left(\mathbf{x}_i^k\right)+\delta' V_l\left(\mathbf{x}\right)\sum_{l\in M_i^k}\theta\left(J_l^R\right)g_{il}\left(\mathbf{x}_i^k\right)\right\} \quad (31)$$

Where $V_a\left(\mathbf{x}\right)$ is the variance matrix from anchor a and $V_l\left(\mathbf{x}\right)$ is the variance matrix from unknown node l.

From the formula (31), the confidence is further expanded to formula (32), (33) and (34).

$$g_{k|k-1}\left(\mathbf{x}_i^k\right) \triangleq -\frac{1}{2}\left(\mathbf{x}_i^k - u_i^{k|k-1}\right)^T \left(V_i^{k|k-1}\right)^{-1}\left(\mathbf{x}_i^k - \mathbf{u}_i^{k|k-1}\right) \quad (32)$$

$$g_{ia}\left(\mathbf{x}_i^k\right) \triangleq \frac{\mathbf{d}_{i\leftarrow a}^k}{\left(\sigma_{ia}^k\right)^2}\left\|\mathbf{u}_a^k - \mathbf{x}_i^k\right\| - \frac{1}{2\left(\sigma_{ia}^k\right)^2}\left\|\mathbf{u}_a^k - \mathbf{x}_i^k\right\|^2 \quad (33)$$

$$g_{il}\left(\mathbf{x}_i^k\right) \triangleq \int \hat{b}\left(\mathbf{x}_l^k\right)\left(\frac{\mathbf{d}_{i\leftarrow l}^k}{\left(\sigma_{il}^k\right)^2}\left\|\mathbf{x}_l^k - \mathbf{x}_i^k\right\| - \frac{1}{2\left(\sigma_{il}^k\right)^2}\left\|\mathbf{x}_l^k - \mathbf{x}_i^k\right\|^2\right) \quad (34)$$

In formula (32), (33) and (34), $g_{k|k-1}\left(\mathbf{x}_i^k\right)$ is the message from last time. $g_{ia}\left(\mathbf{x}_i^k\right)$ is the message from anchors. $g_{il}\left(\mathbf{x}_i^k\right)$ is the message from other unknown nodes. $V_i^{k|k-1}$ is the variance matrix from last time.

However the confidence $b\left(\mathbf{x}_i^k\right)$ is impeded into the Gaussian form by the distance computation $\left\|\mathbf{u}_a^k - \mathbf{x}_i^k\right\|$ and $\left\|\mathbf{u}_l^k - \mathbf{x}_i^k\right\|$. To linearize the distance formula, $\left\|\mathbf{u}_a^k - \mathbf{x}_i^k\right\|$ and $\left\|\mathbf{u}_l^k - \mathbf{x}_i^k\right\|$ are expanded around $\tilde{\boldsymbol{\mu}}_i^k$ and $\left(\tilde{\boldsymbol{\mu}}_i^l, \tilde{\boldsymbol{\mu}}_l^k\right)$ with second-order Taylor expansion, respectively. The linear confidence is shown in formula (35).

$$\hat{b}\left(\mathbf{x}_i^k\right) \propto \exp\left\{-\frac{1}{2}\left(\mathbf{x}_i^k\right)^T\left(\hat{V}_i^k\right)^{-1}\mathbf{x}_i^k + \left(\mathbf{x}_i^k\right)^T\left(\hat{V}_i^k\right)^{-1}\hat{\mathbf{u}}_i^k\right\} \quad (35)$$

The variance and mean value with punctuation function and judgment factor are as follows.

$$\hat{V}_i^k = \left\{\left(V_i^{k|k1}\right)^{-1} + \delta V_a(x)\sum_{a\in A_i}\theta\left(J_a^R\right) \times\left(\frac{1}{\left(\sigma_{ia}^k\right)^2}I - \frac{\mathbf{d}_{i\leftarrow a}^k}{\left(\sigma_{ia}^k\right)^2}\nabla_{F_{ia}}^2\right) + \delta V_l(x)\sum_{l\in M_i^k}\theta\left(J_l^R\right) \times\left(\frac{1}{\left(\sigma_{il}^k\right)^2}I - \frac{\mathbf{d}_{i\leftarrow l}^k}{\left(\sigma_{il}^k\right)^2}Q\right)\right\}^{-1} \quad (36)$$

$$\hat{\boldsymbol{\mu}}_i^k = \hat{V}_i^k\left\{\left(V_i^{k|k-1}\right)^{-1}\boldsymbol{\mu}_i^{k|k-1}\right\} + \delta V_a(x)\sum_{a\in A_i^k}\theta\left(J_a^R\right) \times\left(\frac{1}{\left(\sigma_{ia}^k\right)^2}\boldsymbol{\mu}_a^k - \frac{\mathbf{d}_{i\leftarrow a}^k}{\left(\sigma_{ia}^k\right)^2}\left(\nabla_{F_{ia}} - \nabla_{F_{ia}}^2\tilde{\boldsymbol{\mu}}_i^k\right)\right) + \delta V_l(\mathbf{x}) \times\sum_{l\in M_i^k}\theta\left(J_l^R\right)\left(\frac{1}{\left(\sigma_{il}^k\right)^2}\tilde{\boldsymbol{\mu}}_l^k + \frac{\mathbf{d}_{i\leftarrow l}^k}{\left(\sigma_{il}^k\right)^2}\left(\frac{\partial F_{il}}{\partial \mathbf{x}_i^k} - Q\tilde{\boldsymbol{\mu}}_i^k\right)\right) \quad (37)$$

Where $F_{ia} \triangleq \left(\mathbf{x}_i^k\right)\left\|\boldsymbol{\mu}_a^k - \mathbf{x}_i^k\right\|$, $F_{il}\left(\mathbf{x}_i^k, \mathbf{x}_l^k\right) \triangleq \left\|\mathbf{x}_l^k - \mathbf{x}_i^k\right\|$. $\nabla_{F_{ia}}, \nabla_{F_{ia}}^2$ are the first-order gradient and the Hessian matrix of $F_{ia}\left(\mathbf{x}_i^k\right)$ at $\tilde{\boldsymbol{\mu}}_i^k$. $\frac{\partial F_{il}}{\partial \mathbf{x}_i^k}$ is the first-order partial derivative of $F_{il}\left(\mathbf{x}_i^k, \mathbf{x}_l^k\right)$ around $\left(\tilde{\boldsymbol{\mu}}_i^l, \tilde{\boldsymbol{\mu}}_l^k\right)$. Besides, $Q \triangleq \left(\partial/\partial \mathbf{x}_i^k\right)\left(\partial F_{il}/\partial \mathbf{x}_i^k\right)$.

According to the formula (36) and (37), the unknown node obtains its mean value and variance. These results update the node position relationship. Therefore the unknown node can adjust the position to approach the true value by iteration. In this process, each iteration needs bounding box to correct the deviation. If the position is beyond the bounding box, it means that the large error exists in correction phase. Therefore the center of bounding box is set as the corrected position in this iteration. After finite times of iteration, the position with largest confidence is the final result.

V. SIMULATION AND RESULT

This section presents some measurements that compare the performance of proposed method and other methods in different scenarios. The performance measurements are produced through simulation. Increasing density of anchors or frequency of location announcements should improve accuracy, but the tradeoffs need to be understood to determine appropriate deployment parameters. This section evaluates the proposed technique by measuring how its estimated position errors vary with network and algorithm parameters.

For all experiments, sensors are randomly and uniformly distributed in $100m \times 100m$ field where no obstacles are arranged. The communication module in the sensor node is Zigbee technology. We assume that the Zigbee technology works in frequency channel of 2.4 Hz where the technology has excellent anti-interference capacity. Meanwhile DDDS technology is used in Zigbee to further lower the interference. Therefore, we assume that the simulation environment has no or low level of interference which hardly impact on the communication of sensor nodes. Instead of choosing a certain speed for each destination, all the nodes and anchors randomly vary their speed during each movement. We assume nodes are unaware of their speed and direction, but have a known maximum speed $v_{\max}$. Node can judge if it is within radio range R of another node or not, but it cannot get more precise distance information. In this scenario, we evaluate the performance of the proposed algorithm.

A. ALGORITHM PARAMETERS

Algorithm parameters have big influence on the performance of proposed algorithm. Their selection is explored in this section to further optimize the localization model. The parameters include standard deviation σ_{il} of nodes and iterations k in message passing. In the experiment, we set anchor number $N_A = 10$ and unknown node number $N_M = 90$. The communication radius is $R = 30m$. The maximum speed is $\mathbf{V}_{\max} = 5m/s$.

We firstly analyze the standard deviation σ_{il} of anchors and nodes. It is assumed that the variances of nodes' and anchors' positions in the x-axis and the y-axis to be equal. The standard deviation of anchors is set as $\sigma_{ia} = 1$. The standard deviation

TABLE 1. Parameters in simulation of variance.

Parameter	Value
Area	*100m*100m*
Number of unknown node	*90*
Anchor number of anchor	*10*
Communication radius	*30m*
Max speed	*5m/s*
Distance variance of anchor	$1m^2$
Times of iteration	*10*
Distance variance of unknown node	*1,2,9,25* m^2

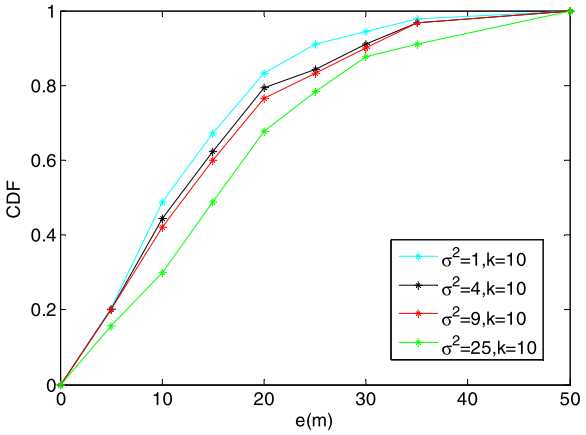

FIGURE 6. CDFs of the algorithm with different deviations.

of unknown nodes is $\sigma_{il} = 1, 2, 3, 5$. In these conditions, the experiment is conducted as the parameters are shown in TABLE 1 and the result is shown in FIGURE 6. Cumulative distribution functions (CDFs) depict the localization error change from 0 m to 50m. From FIGURE 6, 50% error values are between 10 m to 25 m. When the deviation value is larger, the CDFs value is larger and they all converge at 50 m.

TABLE 2 shows the parameters in simulation of iteration and FIGURE 7 shows the CDF result. The CDFs increase as the iteration times varies from 1 to 20. The iteration times from 1 to 10 has a larger growth of CDFs than that from10 to 20. This is due to the convergence of message passing algorithm. If the times of iteration reach 20, the localization error tends to be steady and small.

B. LOCALIZATION ACCURACY OVER TIME

In the mobile WSNs, the node position of each time slot is random and uncertain. These problems may lead to the error accumulation and position deviation. To test the proposed algorithm in the paper, the trajectory errors over time have been depicted in FIGURE 8. The simulation is repeated for 50 times and its error is the average value of the repeated simulation. In the simulation, we set anchor number $N_A = 10$ and node number $N_M = 90$. The communication radius is $R = 30m$. The maximum speed is $V_{\max} = 5m/s$. These parameters are shown in TABLE 3. The error in the FIGURE 8 denotes the average error of all unknown nodes for 100 time slots.

TABLE 2. Parameters in simulation of iteration.

Parameter	Value
Area	*100m*100m*
Number of unknown node	*90*
Anchor number of anchor	*10*
Communication radius	*30m*
Max speed	*5m/s*
Distance variance of anchor	$1m^2$
Distance variance of unknown node	$9\ m^2$
Times of iteration	*1,5,10.15.20*

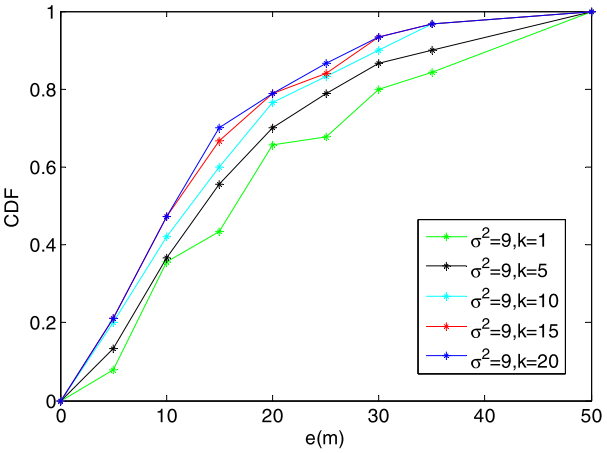

FIGURE 7. CDFs of the algorithm with different iterations.

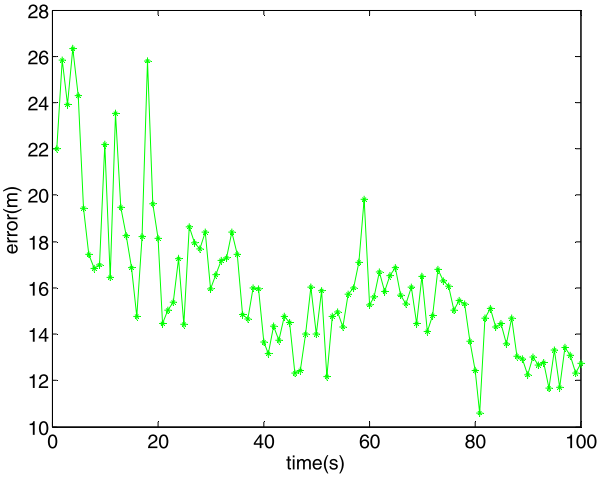

FIGURE 8. Trajectory error of nodes over time.

TABLE 3. Parameters in simulation of time.

Parameter	Value
Area	*100m*100m*
Number of unknown node	*90*
Anchor number of anchor	*10*
Communication radius	*30m*
Max speed	*5m/s*
Distance variance of anchor	$1m^2$
Distance variance of unknown node	$9\ m^2$
Times of iteration	*10*

FIGURE 8 shows the error change from initial localization to 100*th* localization. It can be seen that most of errors are between 14m to 22m and the biggest error doesn't exceed 28m. The error range is acceptable for mobile WSN Localization. In FIGURE 8, the errors fluctuate widely in the first half period of time and errors are relatively large. In the last half period of time, the errors tend to be stable and decrease. This trend indicates that the localization algorithm performs better over time. The reason for the performance is that localization depends on the trajectory prediction at first. Due to the unknown speed and direction, the prediction may be imprecise. In the last period of time, the observation and correction from neighboring nodes contribute to the localization result which helps improve the accuracy. The localization accuracy over time shows that the proposed method in the paper is applicable.

C. LOCALIZATION ACCURACY WITH DIFFERENT MAX SPEED

Varying node speed is similar to varying the time between location announcements. If announcements between nodes are more frequent, localization result is more accurate. However, the communication overhead also increases. Max speed denotes the maximum speed in the mobility of nodes. Nodes move with random speed but their speed doesn't exceed the max speed. In this section, we study the influence of speed when both nodes and anchors have an identical maximum speed. In the experiments, node speeds are distributed between 0 and $v_{\max}$ by random waypoint mobility model. We set anchor number $N_A = 10$ and node number $N_M = 90$. The communication radius is $R = 30m$. These parameters are shown in TABLE 4 and the CDFs with different max speeds have been shown in FIGURE 9.

Node speed impacts the localization process in two ways. The increased speed makes the predicted locations less accurate since the next possible locations fall into a larger region. On the other hand, faster movement leads to more new observations in each time step, so the probability density function of distance is fuzzier. As shown in FIGURE 9, the CDFs decrease when the max speed becomes larger. Both the inaccurate prediction and the larger observation region lead to the lager error. The localization errors drop fast as node speeds decrease from 8m/s to 2m/s. It means the max speed has big influence on the localization accuracy. However

TABLE 4. Parameters in simulation of max speed.

Parameter	Value
Area	*100m*100m*
Number of unknown node	*90*
Anchor number of anchor	*10*
Communication radius	*30m*
Distance variance of anchor	$1m^2$
Distance variance of unknown node	$9\ m^2$
Times of iteration	*10*
Max speed	*2,4,8,10,20 m/s*

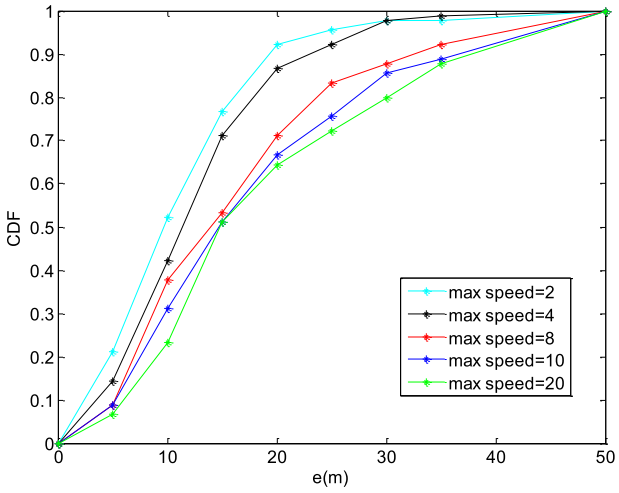

FIGURE 9. CDFs of the algorithm with different max speeds.

TABLE 5. Parameters in simulation of node density.

Parameter	Value
Area	*100m*100m*
Communication radius	*30m*
Distance variance of anchor	$1m^2$
Distance variance of unknown node	$9\ m^2$
Times of iteration	*10*
Max speed	*5 m/s*
Number of unknown node	*45,90,180,.450*
Anchor number of anchor	*5,10,20,50*

the CDFs don't decrease much as the max speed varies from 8m/s to 20m/s. Actually, the large max speed may lead to the fast increasing of localization error especially when max speed is more than 10m/s. The problem has been solved by the bounding box proposed in the paper. The bounding box avoids the gross error and position deviation. It makes sure that the errors in all max speeds are acceptable.

D. LOCALIZATION ACCURACY WITH DIFFERENT DISTRIBUTION PARAMETERS

Node density and anchor proportion are two distribution parameters which have influence on the performance of localization algorithm. To further analyze the influence, the simulations are designed. They are conducted in the $100m \times 100m$ square where the nodes move with the max speed of 5m/s. The influence of node density is firstly analyzed as shown in FIGURE 10 and parameters are shown in TABLE 5.

Node density is the average node number in per square meter. In the fixed area, total number of nodes is 50, 100, 200 and 500. Correspondingly, node density is 0.5, 1, 2 and 5. FIGURE 10 shows that CDFs are highest when node density is 5 and CDFs are lowest when node density is 0.5. CDFs drop as node density decreases. Node density impacts the localization in two ways. The distance estimation is based on the statistical probability and node distribution. Large sample of data collection helps improve accuracy of distance

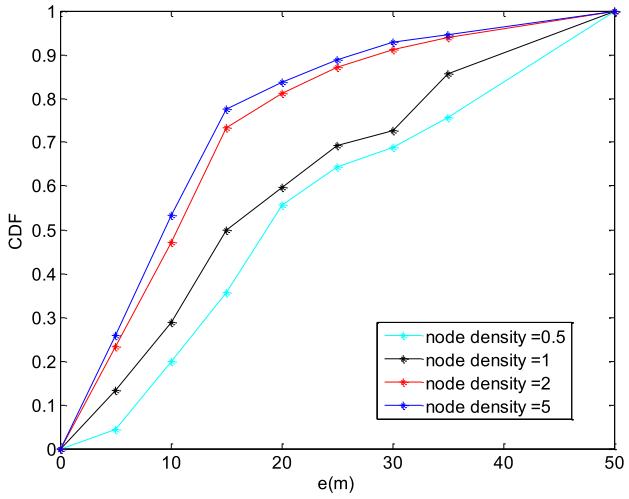

FIGURE 10. CDFs of the algorithm with different node densities.

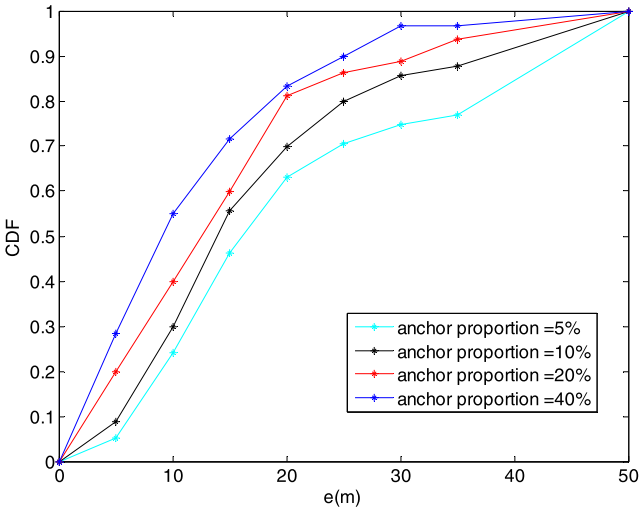

FIGURE 11. CDFs of the algorithm with different anchor proportions.

TABLE 6. Parameters in simulation of anchor proportion.

Parameter	Value
Area	*100m*100m*
Communication radius	*30m*
Distance variance of anchor	$1m^2$
Distance variance of unknown node	$9\ m^2$
Times of iteration	*10*
Max speed	*5 m/s*
Number of unknown node	*95,90,80,.60*
Anchor number of anchor	*5,10,20,40*

TABLE 7. Parameters in simulation of methods.

Parameter	Value
Area	*100m*100m*
Number of unknown node	*90*
Anchor number of anchor	*10*
Communication radius	*30m*
Max speed	*5m/s*
Distance variance of anchor	$1m^2$
Distance variance of unknown node	$9\ m^2$
Times of iteration	*10*

estimation. On the other hand, more nodes can better coordinate the unknown node position. The estimated position approaches the real position more. Therefore, the localization result is more accurate in the condition of high node density.

Anchor proportion is the percentage of anchors in all anchors and unknown nodes. Because anchor obtains its own position by measurement devices, high anchor proportion would provide more reference for unknown nodes. FIGURE 11 shows the localization accuracy comparison in different anchor proportions and TABLE 6 shows the parameters of simulation. In experiment, the node density is 1 and the communication radius is 30m. We compare the localization results for 5%, 10%, 20% and 40% of anchor proportion.

As anchor proportion varies from 5% to 40%, the CDFs increase. For low proportion, the unknown nodes get less information. It is difficult to abstract the relative position information from sparse anchors. The sparse anchors also lead to unavailability and uncertainty of bounding box. These problems cause the low accuracy in low proportion. As the anchor proportion increase, sparsity of anchors is avoided. More useful information contributes to the localization process, so the accuracy improves.

FIGURE 10 and FIGURE 11 show that proposed method in the paper is more suitable for large-scale WSNs. In situation of low node density and anchor proportion, the localization accuracy is also acceptable.

E. ACCURACY COMPARISON OF LOCALIZATION METHODS

This section presents some measurements that compare the accuracy performance of proposed method in the paper (PM), MCL and MCB. We also provide a comparison with two altered versions of Massage Passing (MP) in [13] and [15]. The selected methods above are all suitable for large-scale and mobile WSNs. They are all based on range-free method and don't require extra measurement devices. In the same scenario, the performances are compared through simulations. In this section, we present the CDFs of different methods which effectively illustrate the accuracy. All the methods have been conducted in the same scenario where 90 nodes and 10 anchors are uniformly distributed in the $100m \times 100m$ square. The maximum speed of nodes and anchors are $V_{\max} = 5m/s$. The parameters are shown in TABLE 7 and the localization results of methods are as shown in FIGURE 12.

FIGURE 12 shows that MCL and MCB have close CDFs. Their accuracy is lower compared with other three methods. MCL and MCB are the most popular localization algorithms in mobile WSNs, but their accuracy needs to be improved urgently. VMP and BP-VMP, two altered versions of Massage Passing (MP), make full use of cooperativity, mutual complementary and coherence of adjacent nodes. Their accuracy has been improved a lot. The proposed method in the paper is based on the BP-VMP. Besides, it also considers the

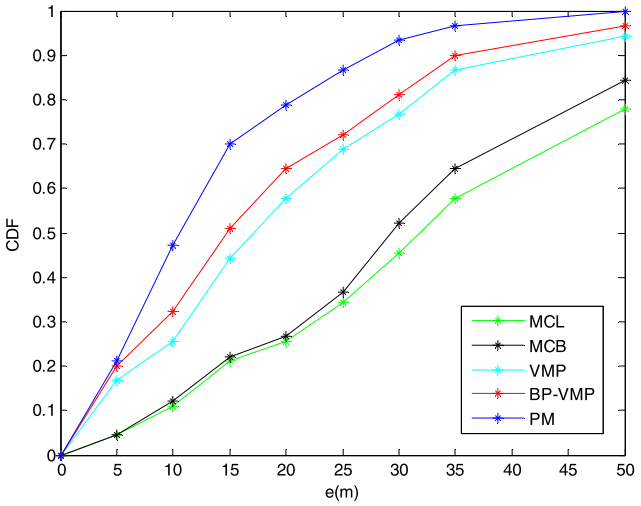

FIGURE 12. Localization method comparison.

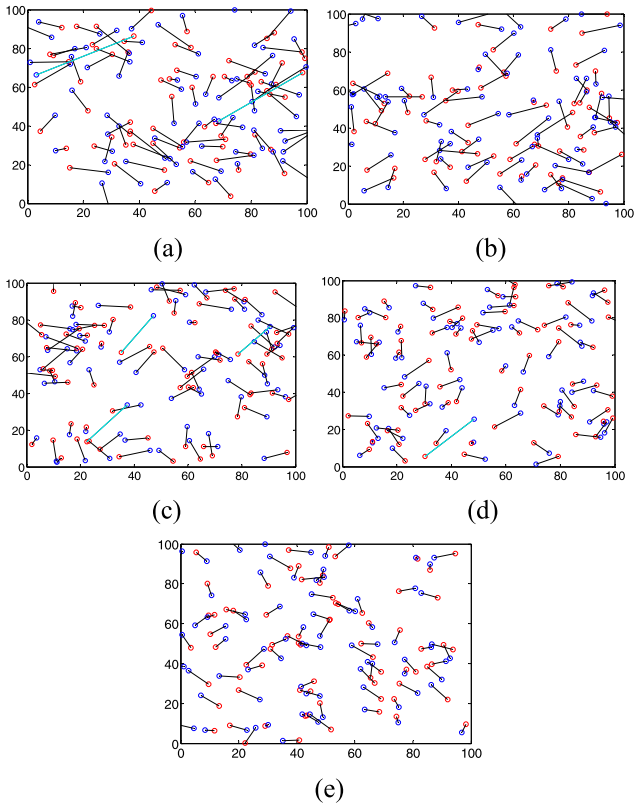

FIGURE 13. Node distribution of five methods. (a) MCL. (b) MCB. (c) VMP. (d) BP-VMP. (e) PM.

boundary constraints and draws support of particle filter from MCL and MCB. The localization result of proposed method in the paper improves the accuracy by 50%. The constraints also help fast convergence so that less computation is conducted.

To intuitively show the localization result, the node distribution is drawn in FIGURE 13. The blue dots are the real positions of the nodes and the red dots are the estimated positions of nodes. The black line is the error of estimated positions of nodes. The blue line is the gross error of estimated positions of nodes. The node distribution of each method is selected from one simulation at the same time slot.

We analyze the node distribution from localization error and gross error. The black line describes the range of error. Because the average error of PM is smallest among five methods, the lines of other four methods are mostly longer than PM. In FIGURE 13(e), the back dots and red dots are close and some of them are nearly coincident. It means the proposed method improves the localization performance. It is more suitable for WSN localization. In addition, MCB and PM don't have blue lines. MCL has two blue lines, VMP has three blue lines and BP-VMP has one blue line. It means the PM outperforms in the prevention of gross error. The bounding constrains proposed in the paper contribute to avoid gross error. It corrects the gross error timely, so large deviation of estimated positions is avoided.

TABLE 8. Computation complexity comparison.

Algorithm	Complexity
MCL	$O(N_p)$
MCB	$O(N_p)$
VMP	$O(N_{i,k}+A)$
BP-VMP	$O(N_{i,k}+A)$
PM	$O(N_{i,k}+B)$

F. COMPLEXITY ANALYSIS

The localization accuracy is compared among MCL, MCB, VMP, BP-VMP and the proposed method. These methods are all simulated in the same scenario. FIGURE 12 shows that proposed method outperforms in the accuracy, but we should make sure that the complexity of the proposed method is acceptable. This section presents the complexity analysis of five methods in the section E. TABLE 8 shows the computational complexity of five methods.

From TABLE 8, the complexities of MCL and MCB are mainly determined by sampling particles N_p. The complexity of VMP, BP-VMP and PM are mainly determined by the number of its neighbors $N_{i,k}$. In the paper, sensors just exchange the mean vector and covariance matrix of their position instead of a huge number of particles, so $N_{i,k} \ll N_p$. Moreover, A, B are the computational complexity of prediction phase and they are almost the same. Therefore, PM doesn't add extra computation complexity. Considering the application of second-order Taylor expansion, its computational complexity is also decreased. The analysis shows that the computational complexity of proposed method is acceptable.

G. ADVANTAGE COMPARISON OF LOCALIZATION METHODS

Different from comparison in section E, this section compares advantages of localization methods. We select the MCL, BP-VMP in paper [36] and LS cooperative localization in paper [22] to compare the proposed method in

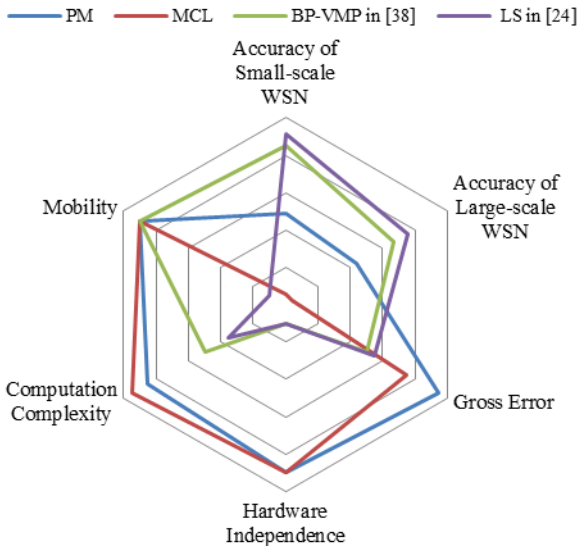

FIGURE 14. Radar chart of localization performance.

accuracy of small and large scale WSN, gross error, hardware independence, computation complexity and mobility. The comparison result is shown in FIGURE 14. The accuracies of small and large scale WSN describe the localization result in different scenarios. The node distribution area of small scale WSNs is $30m \times 30m$. The node distribution area of large scale WSNs is $500m \times 500m$. When the localization error is the smallest among four methods, the radar value of this method is largest and it approaches 1. When the localization error is the largest among four methods, the radar value of this method is smallest and it approach 0. Gross error describes the occurrence probability of gross error. We set the duple average error as the gross error. When the error value is over the duple average error, it belongs to the gross error. If the gross error hardly happens, the radar value of gross error is large. On the contrary, the radar value is small. Hardware independence describes the requirement of hardware equipment. Hardware equipment mainly consists of speed and distance measurement devices. Computation complexity describes the amount of computation. When the amount of computation is small, the radar value of computation complexity is large. Mobility describes the feasibility of the method in localization of mobile WSNs. If the method is feasible in mobile WSN, the radar value of mobility approaches 1, or it approaches 0. The performances of six attributes are reflected in radar chart.

As shown in FIGURE 14, four methods outperforms in different attributes. LS in [22] performs better in both large and small scale WSN, but it isn't feasible in mobile WSNs. The method also depends on range-based methods which have higher hardware cost, and it has higher computation complexity. BP-VMP in paper [36] has higher accuracy, but it depends on TOA method. It means that the accuracy of BP-VMP is improved by adding hardware cost. Because BP-VMP belongs to cooperative localization, it is sensitive to outlier which may lead to catastrophic problem. The radar value of gross error is small. MCL and the proposed method have similar performance in mobility, computation complexity and hardware independence. They all realize localization with less computation and hardware. Compared with MCL, proposed method has higher accuracy and avoids gross error. In radar chart, the area denotes the comprehensive performance. The area is larger, the performance is better. From FIGURE 14, the proposed method in the paper is not the best in accuracy, but it outperforms when six attributes are all considered. Therefore, the proposed method makes a compromise of accuracy and other localization requirement and it is suitable for large-scale WSNs.

VI. CONCLUSION

A cooperative localization algorithm with bounding constraints is proposed for mobile WSNs in the paper. The bounding box limits the predicted node trajectory in the possible area while the judgment factor and punctuation function are introduced in BP-VMP update rule. These improvements realize the calibration of position deviation. Experiments explore the optimal parameter selection and verify the performance of proposed method. The result shows that the proposed method has better error distribution and performs better in different scenarios of node density and anchor proportion. It not only improves the accuracy than regular localization, but also realizes low-cost, large-scale networks localization. The localization algorithm develops cooperative computation and nonlinear dynamics in multi-agent system. Future work may include the relationship between localization and high level of interference associated to WSN signal. We will explore the elimination of interference impact to improve the accuracy of WSN localization.

REFERENCES

[1] C. A. Trasviña-Moreno, R. Blasco, M. Álvaro, R. Casas, and A. Trasviña-Castro, "Unmanned aerial vehicle based wireless sensor network for marine-coastal environment monitoring," *Sensors*, vol. 17, no. 3, pp. 460–469, Mar. 2017.

[2] F. Viani, P. Rocca, M. Benedetti, G. Oliveri, and A. Massa, "Electromagnetic passive localization and tracking of moving targets in a WSN-infrastructured environment," *Inverse Problems*, vol. 26, no. 7, pp. 74–82, Jul. 2015.

[3] Y. Zhang, S. Xing, Y. Zhu, F. Yan, and L. Shen, "RSS-based localization in WSNs using Gaussian mixture model via semidefinite relaxation," *IEEE Commun. Lett.*, vol. 21, no. 6, pp. 1329–1332, Jun. 2017.

[4] V. Henriques and R. Malekian, "Mine safety system using wireless sensor network," *IEEE Access*, vol. 4, pp. 3511–3521, Mar. 2016.

[5] Z. Sheng, C. Mahapatra, and C. Zhu, "Recent advances in industrial wireless sensor networks towards efficient management in IoT," *IEEE Access*, vol. 3, pp. 622–637, May 2015.

[6] A. E. Assaf, S. Zaidi, and S. Affes, "Robust ANNs-based WSN localization in the presence of anisotropic signal attenuation," *IEEE Wireless Commun. Lett.*, vol. 5, no. 5, pp. 504–507, May 2016.

[7] J. Liu, Z. Wang, M. Yao, and Z. Qiu, "VN-APIT: Virtual nodes-based range-free APIT localization scheme for WSN," *Wireless Netw.*, vol. 22, no. 3, pp. 867–878, 2016.

[8] S. Tomic, M. Beko, and R. Dinis, "A closed-form solution for RSS/AoA target localization by spherical coordinates conversion," *IEEE Wireless Commun. Lett.*, vol. 5, no. 6, pp. 680–683, Dec. 2016.

[9] S. Tomic, M. Beko, and R. Dinis, "A robust bisection-based estimator for TOA-based target localization in NLOS environments," *IEEE Commun. Lett.*, vol. 21, no. 11, pp. 2488–2491, Nov. 2017.

[10] R. Jiang and Z. Yang, "An improved centroid localization algorithm based on iterative computation for wireless sensor network," *Acta Phys. Sinica*, vol. 65, no. 3, p. 030101, Mar. 2016.
[11] Y. Wang, X. Wang, and D. Wang, "Range-free localization using expected hop progress in wireless sensor networks," *IEEE Trans. Parallel Distrib. Syst.*, vol. 20, no. 10, pp. 1540–1552, Nov. 2008.
[12] L. Hu and D. Evans, "Localization for mobile sensor networks," presented at the 2nd Int. Conf. Mobile Comput. Netw., Philadelphia, PA, USA, Oct. 004.
[13] A. Baggio and K. Langendoen, "Monte Carlo localization for mobile wireless sensor networks," *Ad Hoc Netw.*, vol. 6, no. 5, pp. 718–733, May 2008.
[14] M. Rudafshani and S. Datta, "Localization for mobile sensor networks," presented at the 2nd Int. Conf. Inf. Process. Sensor Netw., Cambridge, MA, USA, Apr. 2007.
[15] J. Yi, S. Yang, and H. Cha, "Multi-hop-based Monte Carlo localization for mobile sensor networks," presented at the IEEE Commun. Soc. Conf., Washington, DC, USA, Jun. 2007.
[16] W. D. Wang and Q. X. Zhu, "RSS-based Monte Carlo localisation for mobile sensor networks," *IET Commun.*, vol. 2, no. 5, pp. 673–681, May 2008.
[17] M. H. Martins, H. Chen, and K. Sezaki, "Orientation tracking-based Monte Carlo localization for mobile sensor networks," presented at the 6nd Int. Conf. Netw. Sens. Syst., Pittsburgh, PA, USA, Jun. 2009.
[18] Z. X. Guan, Y. T. Zhang, and B. H. Zhang, "Voronoi-based localisation algorithm for mobile sensor networks," *Int. J. Syst. Sci.*, vol. 47, no. 15, pp. 3688–3695, Sep. 2016.
[19] H. Rashid and A. K. Turuk, "Dead reckoning localisation technique for mobile wireless sensor networks," *IET Wireless Sensor Syst.*, vol. 5, no. 2, pp. 87–96, Feb. 2015.
[20] N. Piovesan and T. Erseghe, "Cooperative localization in WSNs: A hybrid convex/nonconvex solution," *IEEE Trans. Signal Inf. Process. Netw.*, vol. 4, no. 1, pp. 162–172, Mar. 2016.
[21] S. Schlupkothen, B. Prasse, and G. Ascheid, "Backtracking-based dynamic programming for resolving transmit ambiguities in WSN localization," *Ad Hoc Netw.*, vol. 2018, no. 1, pp. 1–26, Apr. 2018.
[22] T. V. Nguyen, Y. Jeong, H. Shin, and M. Z. Win, "Least square cooperative localization," *IEEE Trans. Veh. Technol.*, vol. 64, no. 4, pp. 1318–1330, Apr. 2015.
[23] S. H. Li and M. Hedley, "New efficient indoor cooperative localization algorithm with empirical ranging error model," *IEEE J. Sel. Areas Commun.*, vol. 33, no. 7, pp. 1407–1417, Jul. 2015.
[24] Á. F. García-Fernández, L. Svensson, and S. Särkkä, "Cooperative localization using posterior linearization belief propagation," *IEEE Trans. Veh. Technol.*, vol. 67, no. 1, pp. 832–836, Jan. 2018.
[25] H. Wymeersch, J. Lien, and M. Z. Win, "Cooperative localization in wireless networks," *Proc. IEEE*, vol. 97, no. 2, pp. 427–450, Feb. 2009.
[26] V. Savic, H. Wymeersch, and S. Zazo, "Belief consensus algorithms for fast distributed target tracking in wireless sensor networks," *Signal Process.*, vol. 95, no. 2, pp. 149–160, Feb. 2012.
[27] V. Savic and S. Zazo, "Reducing communication overhead for cooperative localization using nonparametric belief propagation," *IEEE Wireless Commun. Lett.*, vol. 1, no. 4, pp. 308–311, Aug. 2012.
[28] H. Wymeersch, F. Penna, and V. Savic, "Uniformly reweighted belief propagation for estimation and detection in wireless networks," *IEEE Trans. Wireless Commun.*, vol. 11, no. 4, pp. 1587–1595, Apr. 2012.
[29] T. G. Roosta, M. J. Wainwright, and S. S. Sastry, "Convergence analysis of reweighted sum-product algorithms," *IEEE Trans. Signal Process.*, vol. 56, no. 9, pp. 4293–4305, Sep. 2008.
[30] C. Pedersen and T. Pedersen, "A variational message passing algorithm for sensor self-localization in wireless networks," presented at the 5nd Int. Conf. Inf. Theory, Nice, France, Jun. 2011.
[31] K. Das and H. Wymeersch, "Censoring for Bayesian cooperative positioning in dense wireless networks," *IEEE J. Sel. Areas Commun.*, vol. 30, no. 9, pp. 1835–1842, Oct. 2012.
[32] J. Cui and Z. Wang, "Message passing localization algorithm combining BP with VMP for mobile wireless sensor networks," *IET Commun.*, vol. 11, no. 7, pp. 1106–1113, Jul. 2017.
[33] J. H. Cui, Z. Y. Wang, and F. S. Wang, "Distributed cooperative localization algorithm based on variational message passing for wireless networks," *J. Signal Process.*, vol. 33, no. 5, pp. 662–668, May 2017.
[34] B. Li, N. Wu, H. Wang, P.-H. Tseng, and J. Kuang, "Gaussian message passing-based cooperative localization on factor graph in wireless networks," *Signal Process.*, vol. 111, pp. 1–12, Jun. 2015.
[35] B. Çakmak and D. N. Urup, "Cooperative localization for mobile networks: A distributed belief propagation—Mean field message passing algorithm," *IEEE Signal Process. Lett.*, vol. 23, no. 6, pp. 828–832, Jun. 2016.
[36] W. J. Yuan, N. Wu, and B. Etzlinger, "Cooperative joint localization and clock synchronization based on Gaussian message passing in asynchronous wireless networks," *IEEE Trans. Veh. Technol.*, vol. 65, no. 9, pp. 7258–7272, Sep. 2016.

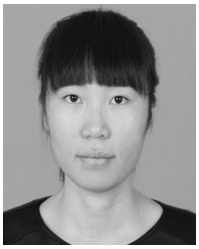

ZHAOYANG WANG received the B.S. and M.S. degrees in control theory and control engineering from Beijing Technology and Business University, Beijing, China, in 2013 and 2016, respectively. She is currently pursuing the Ph.D. degree with the Beijing Institute of Technology, Beijing. Her research interests include wireless sensor networks, localization methods, environmental monitoring, and environment management.

BAIHAI ZHANG received the B.S., M.S., and the Ph.D. degrees in fluid transmission and control from the Harbin Institute of Technology, Heilongjiang, China, in 1988, 1991, and 1994, respectively, and the Post-Doctor degree from the State Key Laboratory of Vehicle Transmission Mechanical Engineering, Beijing Institute of Technology, Beijing, China, in 1997.

From 1997 to 2004, he was a Research Assistant with the Princeton Plasma Physics Laboratory. Since 2004, he has been a Professor with the School of Automation, Beijing Institute of Technology. He was a Senior Visiting Scholar at Michigan State University, USA, in 2001, and was a Visiting Scholar at the University of the West of England, U.K., in 2006. His current research interests include modeling and simulation of complex electromechanical systems, wireless sensor networks, and multi-agent control systems.

XIAOYI WANG received the B.S. degree in physics and electro engineering from Shenyang Ligong University in 2000, the M.S. degree in physics and electro engineering from Shanxi University in 2003, and the Ph.D. degree in control theory and control engineering from the Beijing Institute of Technology, Beijing, China, in 2006.

From 2006 to 2012, he was an Associate Professor with Beijing Technology and Business University. Since 2012, he has been a Professor with Beijing Technology and Business University. Her research covers a variety of areas in water resources protection, modeling, optimization, and simulation of environmental monitoring.

SENCHUN CHAI received the B.S. and M.S. degrees from the Beijing Institute of Technology, Beijing, China, in 2001 and 2004, respectively, and the Ph.D. and Post-Doctor degree in advanced engineering from the University of Glamorgan, U.K., in 2007 and 2009, respectively.

From 2009 to 2010, he was a Visiting Scholar with the University of Illinois, USA. Since 2010, he has been an Associate Professor with the School of Automation, Beijing Institute of Technology. His current research interests include network control, multi-agent, and flight control.

YUTING BAI received the B.S. and M.S. degrees in control theory and control engineering from Beijing Technology and Business University, Beijing, China, in 2012 and 2015, respectively. He is currently pursuing the Ph.D. degree with the Beijing Institute of Technology, Beijing. His research interests include environmental monitoring, information fusion, and environment management.